# Towards the development of a humanoid arm by minimizing interaction forces through minimum impedance control *

**Jaydev P. Desai**
MEM Department, 2-115
3141 Chestnut Street
Drexel University
Philadelphia, PA 19104, USA

**Robert D. Howe**
Div. of Eng. and Appl. Sciences
321 Pierce Hall, 29 Oxford Street
Harvard University
Cambridge, MA 02138, USA

## 1   Abstract

*In this paper, we present the results from our work in the development of a robotic arm with minimal impedance. The development of such an arm is useful for gentle exploration of unknown objects in unstructured environments. Similar to a human, the robotic arm should minimize the contact forces in the event of unanticipated contact with unknown objects in the absence of visual feedback. To accomplish this, our strategy is to develop a good model of the robotic system so that we can use low gains which in turn will lead to low impedance and hence low contact forces in manipulation tasks in unstructured environments. The novel idea about this paper is to demonstrate how good modeling and feedforward compensation can result in low interaction forces without any external force sensing. We present numerous experimental results to demonstrate the validity of our model and approach.*

## 2   Introduction

One of the most useful human manipulation capabilities is the ability to use minimum forces to accomplish a task. An example is grasping an unknown object in an unstructured environment where little visual information is available. As the hand approaches the object, the fingers are soft, so that even though the position of the object is uncertain, unexpected contact will generate little force. This minimizes the likelihood that the object will be disturbed or that the hand will be injured. Later, as the object is firmly grasped, the stiffness of the fingers increases to maintain good control of the object's position as it is manipulated.

This capability is founded on a number of design, control, and sensing mechanisms of the hand. The mechanical impedance of the hand and arm are low before contact to minimize interaction forces. This is due to both the soft tissue covering the fingers

[1] and the compliance at the joints [2]. In both cases, the tissue and joint stiffness increases in proportion to the applied force, so that before contact the stiffness is low, minimizing the ensuing interaction forces. Other important mechanisms include visual sensing to determine approximate object location and size, and tactile sensing to detect the location of contact with the object.

The goal of this paper is to demonstrate the methodology and results of our approach on the development of a humanoid arm using the Whole Arm Manipulator (WAM) robot. Through careful modeling and parameter estimation, we have been able to vary the impedance of the robotic arm from being very gentle to very stiff, thereby accomplishing a variable dynamic range of impedances similar to a human arm. We are aiming to perfect the performance of this robotic arm for a wide variety of tasks commonly carried out by humans from simple gentle probing to complex manipulation and reaching tasks. In our initial stage, we are working to create robotic systems that can perform simple grasping and manipulation operations on a range of objects in unstructured environments. Our approach emulates the mechanisms enumerated above, including variable manipulator impedance and simple visual and contact sensing. In this paper, we explore one aspect of these systems: the ability to control a manipulator to minimize interaction forces in the initial "groping" phase of acquiring unknown objects. This requires the ability to move the manipulator through space with low impedance but with reasonable positional accuracy. This precludes conventional position control methods where high feedback gains are used to minimize position errors, because these high gains also produce high impedance. Our solution is to use a model-based approach, where the model predicts the manipulator torques required to follow the desired trajectory, so that low feedback gains produce low impedance in the event of unanticipated contact.

In addition to a low impedance position controller, the manipulator mechanism itself must also have intrinsically low impedance. Highly geared manipulators cannot be backdriven by contact forces, so they must rely on feedback from sensor signals to drive

the motors to emulate low interaction impedance. While this approach can achieve some measure of success, the use of a compliant manipulator eliminates the need for contact sensing and guarantees good performance even in the presence of sensor noise or failure.

This approach is a straightforward extension of model-based impedance control with, however, a different focus. The role of dynamic models in controlling position in free space has largely been aimed at improving precision and speed [3, 4]. In impedance control, dynamic models have often been used to modify the apparent impedance of the manipulator in the contact phase [3, 5]. Here we aim to use the dynamic model to achieve good position control in free space while at the same time minimizing the contact impedance and limiting the need for sensing.

Research on controlling the forces generated upon contact has often been termed "impact control". In these studies, the focus is often on switching between different controllers for the contact phase, and the use of proximity and/or force sensors to anticipate and control the impact (e.g. [6, 7, 8, 9]). While these approaches have achieved good results, the goal here is to create a controller for use in the free motion phase that does not use sensor feedback to minimize forces in the event of unanticipated contact. This approach improves robustness by eliminating sensors from the control loop, but still results in low interaction impedance through the use of a backdrivable manipulator.

We note that the controller and its implementation on a low-impedance manipulator are just two components of a system that can grasp and manipulate unknown objects in unstructured environments. Other mechanisms, such as soft contact surface coverings and reactive control methods that alter the controller and commanded trajectory in response to contact are also essential. Minimizing the impedance of the manipulator, however, is a robust strategy for avoiding large forces in the inevitable unexpected contacts that could damage the object or the manipulator.

In this study, we design and implement a low impedance position controller and examine its performance in an exploration task that requires contact with an unknown surface. In section 3 we present a description of our experimental testbed, the Whole Arm Manipulator (WAM) (manufactured by Barrett Technology, Cambridge, MA) and describe the modeling procedure for the WAM. In this section, we estimate the inertial parameters of the arm and the friction coefficients. In section 4, we present the results of our experimental system for trajectory following using very low position and velocity gains in the nonlinear impedance control law. Finally, some concluding remarks are made in section 5.
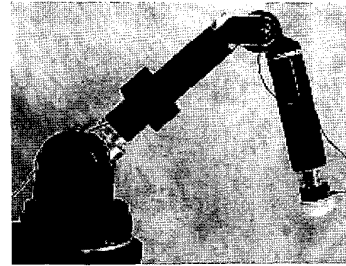


Figure 1: The Whole Arm Manipulator robot (WAM).

## 3 Modeling

The Whole Arm Manipulator (WAM) used in these experiments is a four degree of freedom robot (see Figure 1). The four joints are known as the base, shoulder pitch, shoulder roll, and the elbow joint. The robot is backdrivable, has low friction and intrinsically low impedance. It is thus an ideal robot for developing and implementing the proposed control laws. For these initial experiments, we use the WAM as a 3 DOF arm by "locking" the shoulder roll joint through high gain proportional-plus-derivative (PD) control. This results in a stiffness far higher than the other joints, which are controlled with the minimum impedance controller.

We used a servo controller board with an onboard RISC processor for fast floating point computations (Model DS1103, dSPACE GmbH, Paderborn, Germany). The board has ADC, DAC and incremental encoder interfaces. A six-component force-torque sensor (Dual gain, Gamma F/T 130/10 and 32/2.5, ATI Industrial Automation, Garner, North Carolina) is mounted on the end of the WAM. On this force-sensor we have attached a hemispherical cap as shown in Figure 1, which is used to probe the environment. The force information is not used in the servo loop, but measures contact forces to quantify performance in the exploration task.

### 3.1 Model

Our goal is to devise a model of the manipulator that predicts the joint torques required to drive the robot along a desired trajectory. If this model is accurate, only small feedback torques will be required to overcome modeling errors and unmodeled disturbances. For most of the exploration task, gravity and friction torque will dominate, with dynamic terms (inertia, coriolis, etc.) becoming significant at higher speeds and acceleration. We propose the following terms in the control law:

Dynamic model + Friction + PD = Joint torque + Contact torque

where the Dynamic model includes gravity and

dynamics terms, PD represents error-based feedback terms, and Contact torque represents the contact forces at the tip resolved to the joints. If we can derive sufficiently accurate models of the dynamics and friction, then low PD gains should lead to good trajectory following and low interaction forces. In the following sections, we will derive each term in the above expression and later describe the procedure for parameter identification.

**Dynamic model:**     The schematic of the 3 DOF WAM is shown in Figure 2. Let $m_i$ and $I_i$, denote the mass and inertia tensor (assumed to be diagonal) at the centroid for link $i$ respectively. Similarly let $l_i$ denote the length of link $i$ and $r_i$ denote the distance from the joint to the centroid of link $i$.
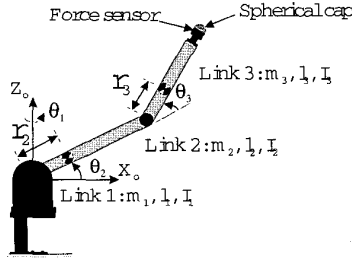


Figure 2: Schematic of the WAM as an anthropomorphic arm.

Based on the notation in the schematic, we can write down the dynamic equations for each link $i = (1, 2, 3)$ of the 3 DOF robot as follows:

$$\sum_{j=1}^{3} H_{ij}(q)\ddot{q}_j + \sum_{j,k=1}^{3} \Gamma_{jk}^i \dot{q}_j \dot{q}_k + G_i(q) = \tau_{i,act} \quad (3.1)$$

where $q = [\theta_1 \ \theta_2 \ \theta_3]^T$ is the $3 \times 1$ vector of generalized coordinates (representing the joint angles), $H_{ij}(q)$ is the $(i, j)$ entry of the configuration dependent $3 \times 3$ inertia matrix, $H(q)$, $\Gamma_{jk}^i$ are the Christoffel symbols corresponding to the inertia matrix $H(q)$, $G(q) = [G_1(q) \ G_2(q) \ G_3(q)]^T$ is the $3 \times 1$ vector of gravitational torques, and $\tau_{act} = [\tau_{1,act} \ \tau_{2,act} \ \tau_{3,act}]^T$ is a $3 \times 1$ vector of joint torques. To rewrite the dynamic equations in vector form, we define the $3 \times 3$ matrix $C(q, \dot{q})$ as follows:

$$C_{ij}(q, \dot{q}) = \sum_{k=1}^{3} \Gamma_{jk}^i \dot{q}_k$$

**Friction:**     Although more elaborate friction models are available [10], we assume a simple model for friction as an initial approach.     We model the Coulomb friction and viscous friction as independent of the joint angle.     We define $D(\dot{q}) = $

$[D_1(\dot{q}) \ D_2(\dot{q}) \ D_3(\dot{q})]^T$ as the $3 \times 1$ vector of viscous and Coulomb friction torques. Also, to prevent the stick-slip situation, we define a threshold velocity band of width $2\delta$ centered around the origin where the frictional torque is parabolic with respect to the joint velocity. Based on this assumption, the expression for friction torque is given by:

$$D_i(\dot{q}) = \begin{cases} V_i\dot{q}_i + S_i sign(\dot{q}_i) & : \ |\dot{q}_i| > \delta \\ V_i\dot{q}_i + \frac{S_i}{\delta}(\frac{sign(\dot{q}_i)\dot{q}_i^2}{\delta} + 2\dot{q}_i) & : \ |\dot{q}_i| \leq \delta \end{cases}$$
$$(3.2)$$

**Interaction with the environment:**     We assume that the desired end-point impedance of the manipulator is given by the expression:

$$M\ddot{X} + B(\dot{X} - \dot{X}_o) + K(X - X_o) = F_e \quad (3.3)$$

where M, B and K denotes the inertia, damping and stiffness in task space coordinates, $X = [x \ y \ z]^T$ is the $3 \times 1$ vector of the task space coordinates, and $X_o$, $\dot{X}_o$ is the desired trajectory and velocity of the tip of the robot. When the manipulator interacts with the environment, an additional interaction torque $\tau_e = J^T(q)F_e$, appears in the dynamic equations, where $J$ is the manipulator Jacobian. Hence the modified dynamic equations taking into account the friction torque and interaction with the environment is given by:

$$H(q)\ddot{q} + C(q, \dot{q})\dot{q} + G_i(q) + D(\dot{q}) = \tau_{act} + \tau_e \quad (3.4)$$

Now the end-effector and joint space velocities are related by:

$$\dot{X} = J\dot{\theta} \quad (3.5)$$

Differentiating Equation (3.5) and substituting for $\ddot{X}$ and $\ddot{\theta}$ from Equation (3.3) and (3.4) and performing some algebraic manipulation, the final expression for the nonlinear feedback law for impedance control in task space coordinates is given by [11]:

$$\tau_{act} = G(q) + C(q, \dot{q})\dot{q} + D(\dot{q}) - HJ^{-1}\dot{J}\dot{q} - J^T F_e$$
$$+ HJ^{-1}M^{-1}F_e + HJ^{-1}M^{-1}K(X_o - X)$$
$$+ HJ^{-1}M^{-1}B(\dot{X}_o - \dot{X}) \quad (3.6)$$

Equation (3.6) represents the various terms in the proposed control law above. The terms $C$, $G$, and $H$ represent the model of the manipulator's dynamics, and contain parameters that are identified experimentally below. The desired interaction stiffness $K$ and damping $B$ multiply the error in position and velocity respectively, and thus correspond to tip space PD feedback gains. Note that in order to achieve an apparent interaction inertia $M$ that is different from the manipulator's inertia, sensing of the interaction force $F_e$ is required [11]. Dependence on this force sensor signal can be avoided by specifying only the stiffness and damping, and leaving the manipulator's intrinsic inertia unchanged. In this case, the force sensor signal drops out of Equation (3.6).

## 3.2 Parameter identification

In this section, we discuss the procedure adopted to estimate the inertial parameters and the friction torque coefficients, $V_i$ and $S_i$. For estimating the inertial parameters, it is advantageous to identify the least number of parameters that need to be estimated. Some of the parameters are completely identifiable, others are identifiable in linear combinations, and some are completely unidentifiable [3]. However, the unidentifiable parameters do not appear in the dynamic equations and hence pose no difficulties. To obtain a reasonably good estimate of the moments of inertia, it is necessary to have a sufficiently rich excitation, *i.e.*, a trajectory with appropriate velocity and acceleration. We used linear combinations of sinusoidal profiles with varying amplitudes and frequencies to generate sufficiently rich excitations. To estimate the inertial parameters, we rewrite the dynamic equations at each data point on the trajectory in the form:

$$\pi_i = \lambda_i \Psi \qquad i = 1, \ldots, N \qquad (3.7)$$

where $N$ is the total number of data points, $\pi_i$ is the $3 \times 1$ vector of actuator torques at data point $i$ as in Equation (3.1) and $\lambda_i$ is a $3 \times 12$ matrix which is a function of the joint angles, angular velocity and angular acceleration. The expression for the unknown parameters $\Psi$ to be estimated is given by:

$$\Psi = [I_{z1} \quad I_{x2} \quad I_{z2} + m_2 r_2^2 \quad I_{y2} + m_2 r_2^2 \quad m_2 r_2 \quad m_3 r_3 \quad I_{x3}$$
$$I_{y3} + m_3 r_3^3 \quad I_{z3} + m_3 r_3^2 \quad V_1 \quad V_2 \quad V_3]^T$$

Since the last link on the WAM is easily removed, we weighed it directly and hence it does not appear in $\Psi$ as an unknown inertial parameter to be estimated. Similarly, we estimated the Coulomb friction coefficients $S_i$ independently and hence they also do not appear in the estimation procedure. The computed values for the Coulomb friction coefficients and the mass of the elbow is substituted in the dynamic Equation (3.7) before estimating $\Psi$.

**Friction estimation:** For estimating the Coulomb friction coefficients, $S_i$ ($i = 1, 2, 3$), we moved the WAM in suitable configurations and locked all the other joints through high-gain PD control except the joint for which friction torque was to be estimated. We also applied the feedforward torque ripple compensation to prevent erroneous values for friction coefficients.

For estimating the Coulomb friction torque coefficient for the base joint, we controlled the second joint of the WAM at $\theta_2 = 90°$ through PD control to minimize the inertia and removed the elbow. We applied torque to the base joint in increments of $1e^{-4}$ and recorded the torque value when there was a deflection from the zero position of the base joint by 2 degrees. The torque value gave us the estimate $S_1$ for the base joint. Similar measurements provided estimates for the other two joints.

**Estimating $\Psi$:** For estimating $\Psi$, $\pi_i$ and $\lambda_i$ are computed at each data point based on the recorded values from the encoders. $\Psi$ is a $12 \times 1$ vector of unknown inertial parameters that needs to be estimated. Based on $\pi_i$ and $\lambda_i$ computed at each data point, we augment Equation (3.7), using the $N$ data points to form a $3N \times 12$ matrix $\Lambda$ and a $3N \times 1$ vector $\Pi$. Note that $\Psi$ is unchanged at all the data points. Hence we can rewrite the augmented form of Equation (3.7) as:

$$\Pi = \Lambda \Psi \qquad (3.8)$$

Since we have carefully chosen the inertial parameters to be identified, $\Lambda$ is full rank and we can compute the pseudo-inverse to estimate $\Psi$. Thus $\Psi$ is given by:

$$\Psi = (\Lambda^T \Lambda)^{-1} \Lambda^T \Pi$$

Using this procedure, we sampled $N = 1600$ data points and the estimated value for $\Psi$ along with the measured values for the mass of the elbow and the Coulomb friction coefficients, $S_i$ ($i = 1, 2, 3$) is: $I_{z1} = 0.0917 Kg - m^2$, $I_{x2} = 0.3331 Kg - m^2$, $I_{z2} + m_2 r_2^2 = 0.4255 Kg - m^2$, $I_{y2} + m_2 r_2^2 = 0.2414 Kg - m^2$, $m_2 r_2 = 0.7853 Kg - m$, $m_3 r_3 = 0.3798 Kg - m$, $I_{x3} = 0.1939 Kg - m^2$, $I_{y3} + m_3 r_3^3 = 0.1022 Kg - m^2$, $I_{z3} + m_3 r_3^2 = 0.1058 Kg - m^2$, $V_1 = 1.1643 N - m/rad/sec$, $V_2 = 1.9823 N - m/rad/sec$, $V_3 = 1.0211 N - m/rad/sec$, $m_3 = 2.7069 Kg$, $S_1 = 1.0233 N - m$, $S_2 = 1.4985 N - m$, $S_3 = 0.5837 N - m$.

# 4 Experiments

## 4.1 Methods

The minimum impedance controller derived in Equation (3.6) above is designed to both accurately follow commanded trajectories in free space and to generate minimal forces upon contact. In this section, we present the results from experiments examining trajectory following and object exploration tasks. In particular, we quantify the effects of impedance, or PD gain, on position accuracy and interaction forces.

## 4.2 Experiment 1

The first experiment characterized trajectory following performance in free space. The robot was commanded to follow two trajectories with different properties. In the first case, the robot end-effector command was a simple sinusoidal profile:

$$x(t) = 0.6 + 0.2 \sin(\frac{\pi}{4} t).$$

In the second case, the robot was required to follow a circular quadrant with unequal axes and a discontinuous velocity profile at the corners. Figure 3 shows trajectory following results for diagonal stiffness and damping matrices (feedback gains) set to 5 N/m and 1.5 N/m/s respectively. Even with these

very low gain values (e.g. a 1 cm displacement generates only 5 grams of restoring force), the robot closely follows the desired trajectory for the sinusoidal motion (Figure 3(a)). The circular quadrant trajectory shown in Figure 3(b) shows the inevitable errors at the corners where the commanded velocities are discontinuous. The commanded velocity had a maximum value of $0.1\pi$. The variation in the rate at which the error dies out along each segment of the trajectory is due to differences in the joint trajectories, which reflects the relative accuracy of the dynamic model parameters (especially friction) for the joints involved. Since we have a reasonable estimate of the parameters, the trajectory profiles were essentially unchanged when we required the trajectories to be followed at higher end-effector velocities.
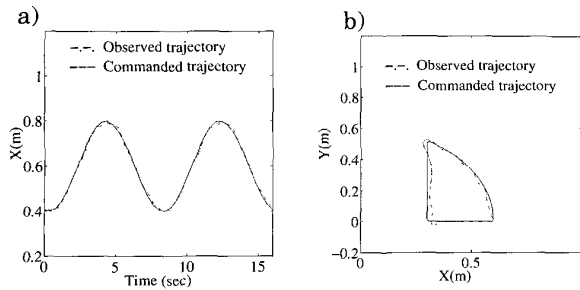
a)                                    b)



Figure 3: a) End-effector following a sinusoidal X motion and b) End-effector following a trajectory with velocity discontinuities.

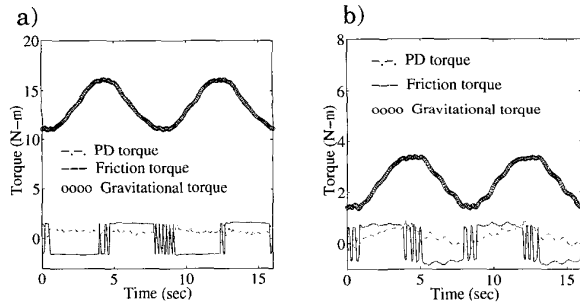a)                                    b)



Figure 4: Torque components for X directional sinusoidal motion for a) joint 2 and b) joint 3.

Finally, to quantify the effects of the dynamic model, we recorded the various torque components generated by the controller for joints 2 and 3 for the trajectory following task of Figure 3(a). As seen in Figure 4, the model-generated gravitational torque for both the joints is substantially higher than both the feedforward friction torque and the error-based PD torque. These plots also show that at the low velocities used in this trajectory profile, the magnitude of the friction torque dominates the PD torque for both the joints. (At the low speeds used here, which

are appropriate for exploratory grasping, the acceleration and velocity dependent dynamic terms are negligible.) The model-based gravitational and friction terms clearly succeed in generating the great majority of the required torque, and enable good trajectory following with low feedback gains.


**Object exploration:** In this experiment, we examined the forces generated by the minimum impedance controller in unanticipated contact. The end effector was required to follow a prescribed exploration probing trajectory and a rectangular wooden object was placed in its planned trajectory path. The periodic trajectory followed by the robot consisted of three components: (1) a vertical downward movement of 10 cm; (2) a vertical upwards movement to where it began the descent; and (3) a movement out from the robot base along the radial direction by 6.67 mm. Once it reached the end of total desired radial travel, the base joint advanced and the robot repeated its periodic movement in the radial direction. Thus as the robot advanced over the wooden block, the spherical cap on the force sensor contacted the block during the descent of the end effector.

Figure 5 shows typical force profiles (filtered at 100 Hz) measured by the sensor for two values of stiffness that differ by a factor of 25. Each contact begins with a fast transient of about 20 N magnitude that is due to the collision of the end effector with the block and is largely independent of the stiffness value. Following this impact, the force magnitude and duration depend on the stiffness setting. Figure 6 plots the measured impulse, i.e. the integral of the force over time, for one cycle of the periodic motion as a function of the stiffness. This figure shows that the impulse varies linearly with stiffness, as predicted for a system where the force is generated by a linear spring. The extrapolated nonzero value of the impulse curve at zero stiffness is due to the impact force, which is a function of the kinetic energy of the robot arm and not stiffness.

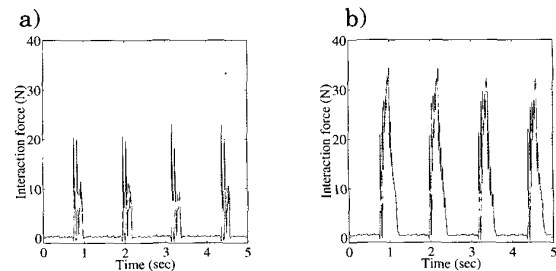a)                                    b)



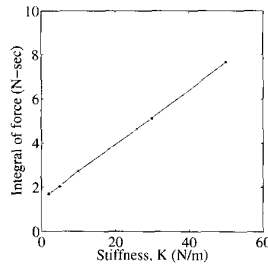Figure 5: Tip forces for a) Lower and b) higher (25 times) stiffness values.

Figure 6: Integral of the interaction force over one period of the trajectory.

## 5 Discussion

This work is part of an effort to develop a robot that can gently interact with objects in unstructured environments, where object size and position may be poorly known. This requires the ability to move the robot to the object with moderate precision but minimal impedance, so that unanticipated contacts do not produce large forces that might disturb the object or damage the robot. The approach implemented here uses a model of the robot's dynamics to predict the joint torques that are needed to follow the trajectory. If the model is accurate, then only small feedback gains are needed to correct residual errors in the model and compensate for disturbances. Because the WAM robot arm is a highly backdrivable, low impedance device, the resulting system has low impedance even without external sensors.

In terms of tuning the controller to particular task requirements, the central tradeoff is between position error and contact force magnitude. This is illustrated by Figure 6: as stiffness increases, the error drops and the contact impulse increases, so appropriate performance may be selected. In unstructured environments where object position is uncertain anyway, there may be no reason to use high gains that might engender high forces.

One interesting question in this context is what limits the minimum practical impedance? There appear to be two factors unrelated to the modeling issues described above. First, external disturbances can apply forces to the arm that by definition cannot be modeled. Feedback is thus required for correction. This is probably not, however, a significant problem in many situations of interest (e.g. indoor settings, passive loads). The second factor that limits impedance is the intrinsic impedance of the manipulator. High impedance devices such as geared robots must use a force sensor to detect contact, and then actively change trajectory to avoid applying large forces. While these systems have met with some success, issues such as servo delays and sensor noise can produce undesirable force transients. Our goal is to develop a system that is intrinsically as low impedance as possible. We will then add external

force sensors and active control mechanisms that respond to contact, and even proximity or visual sensing that can respond before contact. But because the manipulator mechanism and control algorithm have intrinsically low impedance, performance limitations or even failure of these sensors and reactive controllers will not generate high contact forces.

Another passive mechanism that can limit force magnitudes is covering the contact surfaces on the robot arm with soft material. The initial force transients apparent in Figure 5 are due to the dissipation of the robot's kinetic energy in the collision. In this experiment, both the acrylic hemisphere mounted at the end of the arm and the wooden block were hard surfaces, so the contact force rose quickly to a high peak. A layer of rubber would greatly lower the peak magnitude. Once again, however, the impedance of the manipulator (i.e. its inertia) is a key factor in limiting this force, as the kinetic energy is proportional to the inertia. The rubber layer may serve other useful functions as well, such as providing a high-friction gripping surface and a housing for tactile sensors.

## References

[1] D. T. V. Pawluk and R. D. Howe, "Dynamic lumped element response of the human fingerpad," *ASME J. Biomech. Eng.*, vol. 2, pp. 178–184, April 1999.

[2] A. Z. Hajian and R. D. Howe, "Identification of the mechanical impedance at the human finger tip," *ASME J. Biomech. Eng.*, vol. 1, pp. 109–114, Feb 1997.

[3] C. H. An, C. G. Atkeson, and J. M. Hollerbach, *Model based control of a robot manipulator.* Cambridge, MA: MIT Press, 1988.

[4] R. Paul, *Robot manipulators: Mathematics, Programming, and Control.* Cambridge, MA: MIT Press, 1981.

[5] N. Hogan, "Impedance control: An approach to manipulation: Part I - Theory," *ASME Journal of Dynamic Systems, Measurement, and Control*, vol. 107, pp. 1–7, March 1985.

[6] J. K. Mills and D. M. Lokhorst, "Stability and control of robotic manipulators during contact/noncontact task transition," *IEEE Transactions on Robotics and Automation*, vol. 9, pp. 335–45, June 1993.

[7] Y. Wu, T.-J. Tarn, N. Xi, and A. Isidori, "On robust impact control via positive acceleration feedback for robot manipulators," in *Proceedings of IEEE International Conference on Robotics and Automation*, (Minneapolis, MN), pp. 1891–1896, April 1996.

[8] Y. F. Li, "A sensor-based robot transition control strategy," *International Journal of Robotics Research*, vol. 15, pp. 128–136, April 1996.

[9] N. Hogan, "Stable execution of contact tasks using impedance control," in *Proceedings of the 1987 IEEE International Conference on Robotics and Automation*, (Raleigh, NC, USA), pp. 1047–1054, 1987.

[10] B. Armstrong, "Friction: experimental determination, modeling and compensation," in *IEEE International conference on Robotics and Automation*, vol. 3, (Washington, DC, USA), pp. 1422–1427, 1988.

[11] N. Hogan, "Impedance control: An approach to manipulation: Part II - Implementation," *ASME Journal of Dynamic Systems, Measurement, and Control*, vol. 107, pp. 8–16, March 1985.